Implementation of a bound-constrained solver in phase-field modelling of fracture

Rafael G. Bayao[1], Hugo M. Leão[2], Matheus M. Fortes[2], Lapo Gori[2], Roque L. S. Pitangueira[2]

[1]*Mechanical Engineering Undergraduate Course, Federal University of Minas Gerais*
Av. Antonio Carlos, 6627, Pampulha, Belo Horizonte, 31270-901, Minas Gerais, Brazil
rgbayao@gmail.com
[2]*Dept. of Structural Engineering, Federal University of Minas Gerais*
Av. Antonio Carlos, 6627, Pampulha, Belo Horizonte, 31270-901, Minas Gerais, Brazil
hugomleao@yahoo.com.br, matheuseng97@gmail.com, roque@dees.ufmg.br, lapo@dees.ufmg.br

Abstract. In phase-field modelling of fracture, the cracking representation is conditioned by the relation between the displacement field and a phase-field variable that measures the degradation of the material. In this sense, the cracks are modelled as smooth and diffuse according to a group of functions that best represents the geometry of the region where the phenomenon takes place and how the strain energy is degraded during crack propagation. Using a variational formulation of Griffith's criterion, these functions are combined in such a way to attend to the balance laws and the crack irreversibility condition, as well as the bounds of the phase-field variable. The Department of Structural Engineering of the Federal University of Minas Gerais (UFMG) has been currently incorporating, in its open-source software INSANE (Interactive Structural Analysis Environment system), various phase-field models. Nonetheless, the software still has some limitations as the use of some functions may extrapolate the phase-field bounds during solving. The literature has described the use of a bound-constrained solver that can overcome this issue. Therefore, this work proposes the implementation of this solution strategy without the use of any external libraries.

Keywords: phase-field, bound-constrained solver, active-set Newton-Raphson.

1 Introduction

In structural engineering, the prediction and description of crack paths and structural behaviour during fracture have always been a challenge. In this regard, several computational methods have been developed to achieve precision and performance. Particularly in Finite Element Methods, one can invoke models that try to reach this objective by the use of adaptive discontinuous meshes, that cast the crack directly in the arrangement of the elements, and others, by using continuous meshes, with degradation conditions for representing the fracture. For the latter, various physical phenomena or engineering solutions have been incorporated in the literature, as smeared cracking models and damage models. The phase-field modelling of fracture (PFM) is another approach that has gained prominence within the last years.

The PFM approach for the modelling of quasi-static fracture processes has its foundation in Griffith's theory, but with changes regarding the sharpness of the crack. In this sense, opposing to the base theory, the model describes the crack as a smooth region with the degradation magnitude evaluated by a phase-field variable, ϕ. This change is essential to overcome numerical discontinuities that might lead to solution errors.

For solving the PFM different approaches can be invoked from the literature, normally based on monolithic or alternating convergence schemes. In either cases, the main concern of the solving techniques, besides convergence issues, is the imposition of the bound and irreversibility conditions on the phase-field variable. A well-known strategy was developed by Miehe et al. [1], which proposed the use of a historical variable to secure a monotonic evolution of the effective strain energy. This scheme achieves great robustness but is conditioned to the use of a restricted group of functions to ensure the irreversibility condition. In this sense, this restriction leads to problems in relating the model variables with physical quantities as tension stress strength. Farrel and Maurini [2] introduced

another strategy by using a reduced-spaced active set Newton-type solver developed by Benson and Munson [3]. This algorithm allows the use of a wider variety of functions, that along with other definitions, enable a better understanding of the relation between the model and physical properties.

Hence, this works aims to make a new implementation in the INSANE system of the latter mentioned algorithm to allow the study of more recent functions for PFM. Besides the existence of external libraries with great performance, a home-made implementation would grant a better understanding of the steps taken during solving and allow future personalisation of the algorithm for research purposes.

2 Foundation of the Phase-field theory

In general, Griffith's theory problem can be described as a body domain Ω, with an external boundary $\partial\Omega$, a component relative to loading $\partial\Omega_t$, prescribed displacements $\partial\Omega_u$ and a sharp crack Γ, Fig. 1(a). In Phase-field formulation the sharp crack Γ is replaced by a diffuse domain $\mathcal{B}$, as illustrated in Fig. 1(b).

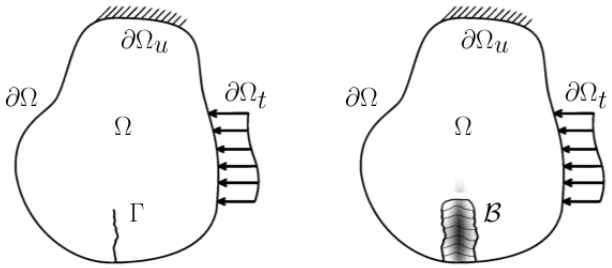

(a) (b)

Figure 1. Problem visual description with (a) sharp crack; (b) diffuse crack;

Griffith's criterion estimate a fracture critical energy by relating the crack surface growth energy (Ψ_c), the strain energy release energy (Ψ_s) and the energy provided by external forces (P_{ext}), eq. (1).

$$E_t(\bar{u}) = \Psi_c + \Psi_s - P_{ext} \tag{1}$$

In order to take into account the diffuse crack region and the phase-field variable, the equations Ψ_c and Ψ_s can be approximated accordingly to eq. (2) and eq. (3), respectively.

$$\Psi_c = \int_\Gamma G_f d\mathcal{A} \approx \int_\mathcal{B} G_f \gamma(\phi, \bigtriangledown\phi) d\mathcal{V} \tag{2}$$

$$\Psi_s = \int_\Omega \psi_0(\underline{\epsilon}) d\mathcal{V} \approx \int_\Omega \psi(\underline{\epsilon}, \phi) d\mathcal{V} \tag{3}$$

where G_f is the critical energy release rate, a material property, and $\gamma(\phi, \bigtriangledown\phi)$ the crack surface density function, which will be explained in Section 2.1.

2.1 Smooth crack representation

As previously explained, the ϕ variable describes the state of degradation of a domain point, therefore it can vary from 0, representing an intact material, to 1, which represents a fully degraded material. Hence, within this approach, Wu [4] described a formulation for γ accordingly to eq. (4):

$$\gamma(\phi, \bigtriangledown\phi) = \frac{1}{C_0}\left[\frac{1}{l_0}\alpha(\phi) + l_0 \left|\bigtriangledown\phi\right|\right] \tag{4}$$

where l_0 represents the crack characteristic length, see fig. 2, α the Geometric Crack Function (GCF) and $C_0 = \int_0^1 \alpha^{\frac{1}{2}}(\phi)d\phi$ a constant relative to the α function chosen. The GCF values must be defined in the range $\alpha(\phi) \in [0, 1]$ and satisfy the properties $\alpha(0) = 0$ and $\alpha(1) = 1$.

One can find several α functions in the literature. For quasi-static fracture problems, the most used functions are the one introduced in Bourdin et al. [5], $\alpha(\phi) = \phi^2$, and the linear approach, $\alpha(\phi) = \phi$ from Pham et al. [6], beside of those, Wu [4] suggests the use of $\alpha(\phi) = 2\phi - \phi^2$ and introduces a general formulation:

$$\alpha(\phi) = \xi\phi + (1 - \xi)\phi^2 \qquad \text{with: } \xi \in [0, 2] \tag{5}$$

The bounds of ξ are essential so the function becomes monotonically crescent. To visualize it better, one may refer to fig. 2 which plots the functions in a unidimensional domain.

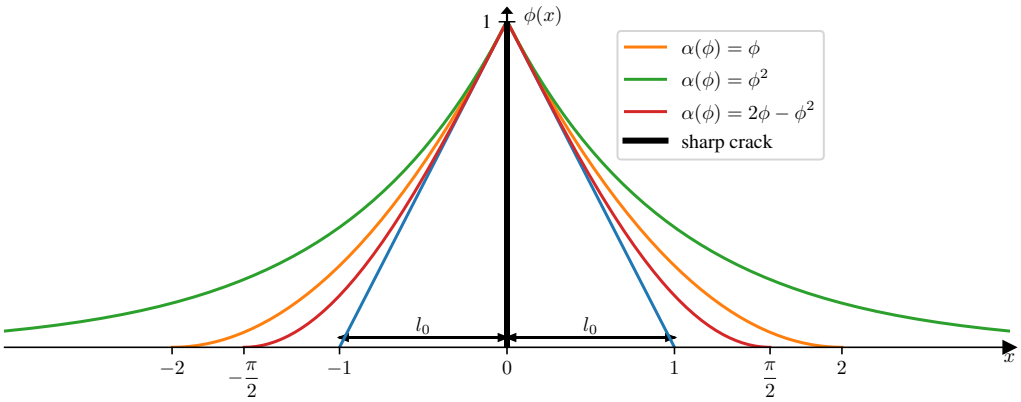

Figure 2. Various GCFs with $l_0 = 1$ and crack in $x = 0$ in a unidimensional domain

2.2 Strain energy degradation

Equation 3 pointed out the necessity to redefine the strain energy density ψ_0 as a function of ϕ, for that purpose, an Energetic Degradation Function (g) is usually defined, which represent mathematically how the degradation affects the region strain energy. The function g is usually implemented as in eq. (6):

$$\psi(\underline{\epsilon}, \phi) = g(\phi)\psi_0(\underline{\epsilon}) \tag{6}$$

There are many energetic degradation functions (EDFs) used in the literature. They must verify, according to Wu et al. [7], the values $g(0) = 1$ and $g(1) = 0$ at the boundaries, which represent respectively an intact and a fully degraded energetic conditions. Besides, it is important that $g'(\phi) < 0$ for $\phi \in (0, 1)$, therefore the equation will be a monotonically decreasing function and that $g'(1) = 0$, to avoid abrupt changes in the function boundary. The EDF which will be used in this work was presented in Wu [4] and can be expressed as:

$$g(\phi) = \frac{(1 - \phi)^p}{(1 - \phi)^p + Q(\phi)} \qquad Q(\phi) = a_1\phi + a_1a_2\phi^2 + a_1a_2a_3\phi^3 \tag{7}$$

The parameters a_1, a_2, a_3 and p in can be related with material properties, e.g. in a one dimensional problem:

$$a_1 = \frac{2E_0G_f}{{f_t}^2} \cdot \frac{\xi}{C_0 l_0} \tag{8}$$

$$a_2 = \frac{1}{\xi}\left[\left(-\frac{4\pi\xi^2 G_f}{C_0 f_t}k_0\right)^{\frac{2}{3}} + 1\right] - (p + 1) \tag{9}$$

$$a_3 = \begin{cases} 0 & p > 2 \\ \dfrac{1}{a_2}\left[\dfrac{1}{\xi}\left(\dfrac{C_0 w_c f_t}{2\pi G_f}\right)^2 - (1+a_2)\right] & p = 2 \end{cases} \tag{10}$$

where ξ is the value of Wu [4] α function, eq. (5), f_t is the material tension strength, k_0 is the function slope at the start of the degradation process and w_c the maximum crack opening displacement reached with residual stress. Both k_0 and w_c correspond to the respective values obtained in a standard tension test simulation and can be related to the aimed softening law desired for the analysis.

3 Bound-Constrained Solver

The herein explained bound-constrained solver is a strategy introduced in Farrel and Maurini [2] to overcome the phase-field variational challenge in dealing with the bound, $\phi \in [0, 1]$ and irreversibility of the phase-field variable, $\dot{\phi} > 0$. The author describes the variational as a mixed complementary problem (MCP), a formulation based in mathematical programming optimisation, and defines the following optimisation conditions for the nodal phase-field variable a_I:

$$\begin{cases} a_{I,n} < a_{I,n+1} < 1 & r_I^\phi = 0 \\ a_{I,n+1} = a_{I,n} & r_I^\phi \leq 0 \\ a_{I,n+1} = 1 & r_I^\phi \geq 0 \end{cases} \tag{11}$$

where $I = 1, 2, 3...$ represents each node in the analysis, a_I is described by the relation $\phi_I = [\mathbf{N}]_I^\phi \, a_I$, in which $[\mathbf{N}]_I^\phi$ is the shape function for the phase-field variable and the node I and r_I^ϕ is the residual of the phase-field variational in finite element method formulation, for further details see Wu et al. [7].

To solve the MCP, Farrel and Maurini [2] suggest the use of the reduced space active-set method from Benson and Munson [3]. It can be done by separating the nodes in active groups, that reached the expected optimisation, and inactive ones, in which will perform a Newton-Raphson type iteration. Furthermore, it is recommended to use a backtracking line search method at the end of each iteration, to improve performance aspects.

The active-set is defined by the group of nodes with $a_{I,n+1} = a_{I,n}$ and $r_I^\phi < 0$ or $a_{I,n+1} = 1$ and $r_I^\phi < 0$. The remaining are labelled as inactive, and iterated over. The solution algorithm is illustrated in fig. 3:

Data: $(\bar{a}_n, \bar{a}_{n+1}^0)$
Result: $(\bar{a}_{n+1}^k)$
while $\left\|\bar{F}_\Theta(\bar{a}_{n+1}^k)\right\| >$ *tolerance* **do**
  Define sets: active ($\mathcal{A}$) and inactive ($\mathcal{I}$);
  Calculates $\left[\mathbf{N}^{\phi\phi}\right]^k$ and $\left[\mathbf{N}^{\phi\phi}\right]_{\mathcal{I}}^k$ by the indices of the sets;
  Calculate the search-direction $\bar{p}_{\mathcal{I}}^{k+1} = \left[\mathbf{N}^{\phi\phi}\right]_{\mathcal{I}}^{-1,k} \cdot \bar{r}_{\mathcal{I}}^{\phi,k}$ and sets $\bar{p}_{\mathcal{A}}^{k+1} = \bar{0}$;
  Find biggest $\mu = \lambda^l < 0$ that solves $\left\|F_\Theta(\pi\left[\bar{a}_{n+1} + \lambda^l \bar{p}^{k+1}\right])\right\| \leq (1 - \tau\lambda^l)\left\|F_\Theta(\bar{a}_{n+1}^k)\right\|$;
  If the line search fails, choose $\mu = \lambda^l$ that leads to the steepest descent;
  Define $\bar{a}_{n+1}^{k+1} = \pi\left[\bar{a}_n^k + \mu\bar{p}^{k+1}\right]$;
  k = k+1;
end

Figure 3. Bound-constrained solver for the n-th step

where $\pi[X]$ is a projector operator and $F_\Theta(X)$ is a restriction operator respectively defined as:

$$\pi[\bar{a}]_l = \begin{cases} 1, \text{ if } a_I \geq 1 \\ 0, \text{ if } a_I \leq 0 \\ a_I \text{ if } 0 \leq a_I \leq 1 \end{cases} \qquad F_\Theta(\bar{a}_{n+1})_I = \begin{cases} r_I^\phi, & \text{for } a_{I,n} < a_{I,n+1} < 1 \\ \min(r_I^\phi, 0), & \text{for } a_{I,n+1} = 1 \\ \max(r_I^\phi, 0), & \text{for } a_{I,n+1} = a_{I,n} \end{cases} \tag{12}$$

4 Numerical Examples

4.1 Shear test

The shear test is a common example in the phase-field literature. The test is illustrated in fig. 4(a), where $\mathcal{S}$ is a predefined crack. Two meshes will be considered for the test, a quadrilateral transfinite with element size of $h = 0.001$ mm and another unstructured mesh with a nodal distance ranging from 0.1 to 0.002 millimetres. The objective is to compare the results of the new implemented solver with the results using historical variable reported in Leão [8] work. Thus, the problem is defined with the following material properties: Young modulus E_0 = 210000 N/mm^2, Poisson's constant ν = 0.2, fracture energy G_f = 2.7 N/mm and l_0 = 0.02 mm. Besides, the equations $\alpha = \phi^2$ and $g = (1-\phi)^2$ by Bourdin et al. [5] were used, together with Miehe et al. [1] constitutive model.

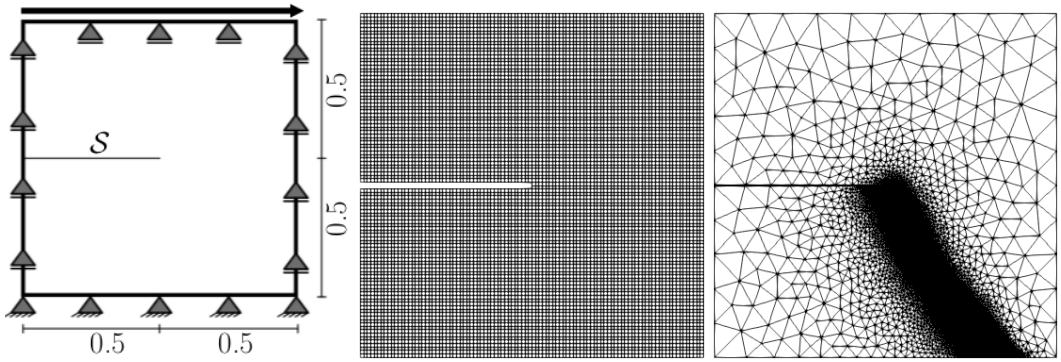

(a) (b) (c)

Figure 4. Shear test: (a) problem model (in millimeters), (b) Q4 structured mesh, (c) T3 unstructured mesh

For the processing parameters, a displacement control strategy was used, where the top-right node performed steps of $1 \cdot 10^{-4}$ mm. For the tolerance, $1 \cdot 10^{-4}$ was set for displacement and phase-field individual control and $1 \cdot 10^{-3}$ for global control.

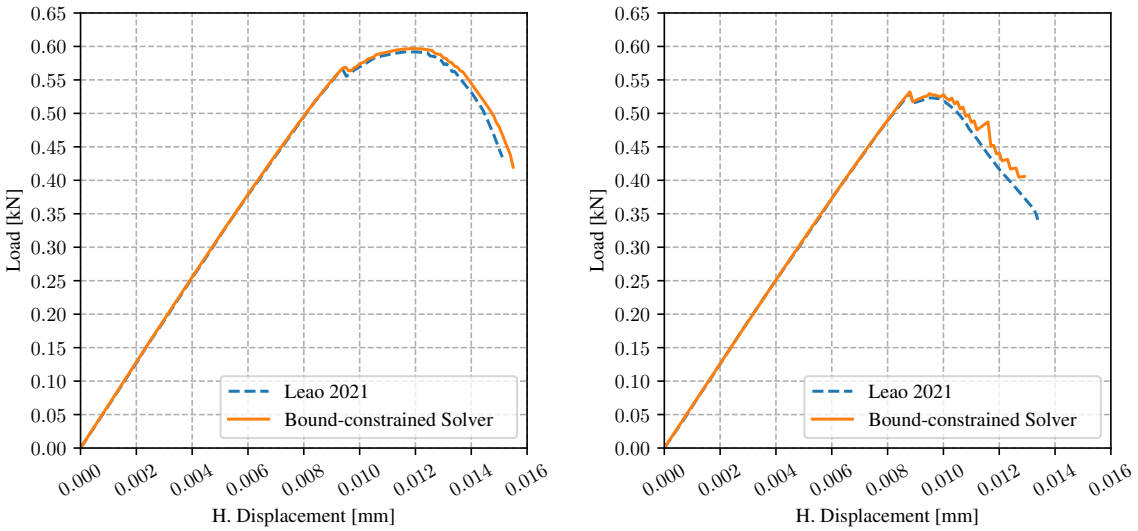

(a) (b)

Figure 5. Displacement of control node (a) in Q4 mesh; (b) in T3 mesh;

The results showed that the new implementation achieves similar results for both meshes. Even though for the triangular unstructured mesh the degradation process didn't perform as smoothly as with the historical variable solver, it still predicted alike shape and maximum load.

4.2 L-shaped panel

The L-shaped panel is a benchmarking test provided with experimental results in the work of Winkler et al. [9]. The example will be performed to compare the PFM results with smeared cracking models results presented in Penna [10]. The analysis is performed in resemblance to the experimental arrangement, illustrated in fig. 6(a), therefore the ground nodes are fixed in both x and y directions. To follow the same model conditions as used by Penna [10], a uniform distributed vertical load was applied at all nodes on the left side of the structure.

As it can be seen, the mesh used in the smeared crack model from Penna [10], fig. 6(b) is far less refined than the one used in the here presented phase-field analysis, fig. 6(c). That is due to model conditions, wherein smeared cracking models, a refinement might lead to numerical errors, and in PFM, it is needed to best represent the GCF. Therefore, a mesh with $h = 50$ mm and with a refinement of $h = 1$ mm in the crack region was used.

For this analysis, the constitutive model and functions of Wu [4] was used. Furthermore, GCF with $\xi = 2$ and two different values for the EDF were set: using Cornelissen's softening law for concrete, thus a_2 = 1.3868 and a_3 = 0.6567, and an Exponential Softening law, with a_2 = 0.1748, a_3 = 0 and p = 2.5, for details about the chosen values refer to Wu [4]. The simulation was performed with the same material properties as in Penna [10]: E_0 = 25850.0 N/mm2, f_t = 2.7 N/mm^2, f_c = 31.0 N/mm^2, G_f = 0.065 N/mm^2 and ν = 0.18. The material was calibrated by the result of a load-displacement traction analysis of a single square element with 1 mm side, fig. 7(a), which led to the use of l_0 = 8.5 mm. An additional simulation was performed with the parameters from Unger et al. [11] that uses Young's modulus E_0=20000.0 N/mm2 and fracture energy G_f = 0.065 N/mm^2, which are different from the original values of the experiment from Winkler et al. [9] but gives a result curve closer to the experimental data.

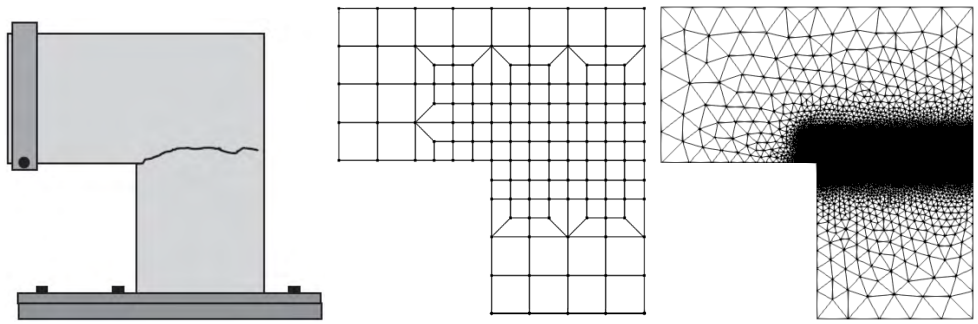

(a) (b) (c)

Figure 6. L-panel test: (a) problem model; (b) Smeared crack mesh; (c) PFM mesh;

For the processing parameters, a displacement control strategy was used, where the top left node performed steps of 0.002 mm in y direction. For the tolerance, $1{\cdot}10^{-5}$ was set for displacements and phase-field individual control and $1{\cdot}10^{-4}$ was set for global control. The results can be seen in the fig. 7(b).

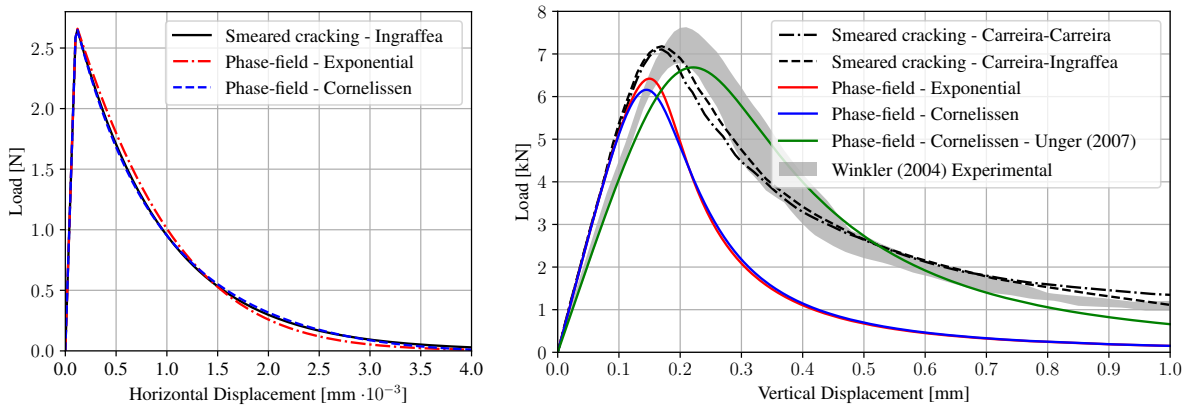

(a) (b)

Figure 7. L-shaped Panel: (a) calibration results; (b) control node displacement within various input parameters;

Figure 7(b) showed that, even though having similar material behaviour, the PFM models performed very unlike the smeared cracking models and the experimental results. It predicted a similar shape for the results but

failed to achieve the maximum load in the experimental range and overestimated the degradation throughout the analysis.

5 Conclusions

The presented data shows that the newly implemented solver can successfully use various formulations of PFM and solve the model respecting the phase-field variable bounds. Although the results in the shear test with triangular unstructured mesh had a descendent region not as smooth as in the historical variable based solver, it could still achieve great similarity in the results.

In the L-Panel experiment, it was possible to notice that the bound-constrained solver was able to handle the newly implemented functions without convergence problems or non-expected results. The shape of the results were in agreement with the experimental data, even though they did not achieve values as good as in the smeared cracking models. Future works may bring up new functions or better ways to calibrate the model to achieve more precise results.

Acknowledgements. The authors gratefully acknowledge the important support of the following Brazilian agencies FAPEMIG (in Portuguese "Fundação Nacional de Amparo à Pesquisa de Minas Gerais" - Grant PPM-00747-18), CNPq (in Portuguese "Conselho Nacional de Desenvolvimento Científico e Tecnológico" - Grants 309515/2017-3) and CAPES (in Portuguese "Coordenação de Aperfeiçoamento de Pessoal de Nível Superior").

Authorship statement. The authors hereby confirm that they are the sole liable persons responsible for the authorship of this work, and that all material that has been herein included as part of the present paper is either the property (and authorship) of the authors, or has the permission of the owners to be included here.

References

[1] C. Miehe, F. Welschinger, and M. Hofacker. Thermodynamically consistent phase-field models of fracture: Variational principles and multi-field fe implementations. *International Journal for Numerical Methods in Engineering*, vol. 83, n. 10, pp. 1273–1311, 2010.

[2] P. Farrel and C. Maurini. Linear and nonlinear solvers for variational phase-field models of brittle fracture. *International Journal for Numerical Methods in Engineering*, vol. 109, pp. 648–667, 2017.

[3] S. J. Benson and T. S. Munson. Flexible complementarity solvers for large-scale applications. *Optimization Methods and Software*, vol. 21, n. 1, pp. 155–168, 2006.

[4] J. Y. Wu. A unified phase-field theory for the mechanics of damage and quasi-brittle failure. *Journal of the Mechanics and Physics of Solids*, vol. 103, pp. 72–99, 2017.

[5] B. Bourdin, G. Francfort, and J. J. Marigo. Numerical experiments in revisited brittle fracture. *Journal of the Mechanics and Physics of Solids*, vol. 48, n. 4, pp. 797–826, 2000.

[6] K. Pham, H. Amor, J.-J. Marigo, and C. Maurini. Gradient damage models and their use to approximate brittle fracture. *International Journal of Damage Mechanics*, vol. 20, n. 4, pp. 618–652, 2011.

[7] J. Y. Wu, Nguyen, V. P., D. Sutula, S. Bordas, and N. C. T. Phase-field modelling of fracture. *Advances in applied mechanics: multi-scale theory and computation*, vol. 52, n. 1, pp. 1–183, 2020.

[8] H. M. Leão. Implementation in insane of the phase-field modelling with fem. Master's thesis, Graduation Programm in Structural Engineering, Federal University of Minas Gerais, Belo Horizonte, MG (Brasil), 2021.

[9] B. Winkler, G. Hofstetter, and H. Lehar. Application of a constitutive model for concrete to the analysis of a precast segmental tunnel lining. *International Journal for Numerical and Analytical Methods in Geomechanics*, vol. 28, pp. 797–819, 2004.

[10] S. S. Penna. *Formulação Multipotencial para Modelos de Degradação Elástica: Unificação Teórica, Proposta de Novo Modelo, Implementação Computacional e Modelagem de Estruturas de Concreto*. PhD thesis, Graduation Programm in Structural Engineering, Federal University of Minas Gerais, Belo Horizonte, MG (Brazil), 2011.

[11] J. Unger, S. Eckardt, and C. Könke. Modelling of cohesive crack growth in concrete structures with the extended finite element method. *Computer Methods in Applied Mechanics and Engineering*, vol. 196, pp. 4087–4100, 2007.